# Experimental Investigation of the Impact of Biogas on a 3 kW Micro Gas Turbine FLOX®-Based Combustor

**Hannah Seliger-Ost*, Peter Kutne, Jan Zanger, Manfred Aigner**
German Aerospace Center
Institute of Combustion Technology
Pfaffenwaldring 38-40
70569 Stuttgart, Germany
Email: hannah.seliger@dlr.de

## ABSTRACT

*The use of biogas has currently two disadvantages. Firstly, processing biogas to natural gas quality for feeding into the natural gas grid is a rather energy consuming process. Secondly, the conversion into electricity directly in biogas plants produces waste heat, which largely cannot be used. Therefore, a feed-in of the desulfurized and dry biogas to local biogas grids would be preferable. Thus, the biogas could be used directly at the end consumer for heat and power production. As biogas varies in its methane ($CH_4$) and carbon dioxide ($CO_2$) content, respectively, this paper studies the influence of different biogas mixtures compared to natural gas on the combustion in a FLOX®-based six nozzle combustor. The single staged combustor is suitable for the use in a micro gas turbine (MGT) based combined heat and power (CHP) system with an electrical power output of 3 kW. The combustor is studied in an optically accessible atmospheric test rig, as well as integrated into the MGT system. This paper focuses on the influence of the admixture of $CO_2$ to natural gas on the $NO_X$ and CO emissions. Furthermore, at atmospheric conditions the shape and location of the heat release zone is investigated using OH* chemiluminescence (OH**

*Address all correspondence to this author.

*CL). The combustor could be stably operated in the MGT within the complete stationary operating range with all fuel mixtures.*

Keywords: combustion, emissions, energy conversion, experimental, fules and combustion, power (co-)generation, flameless oxidation, biogas, FLOX®, micro gas turbine, CHP

## NOMENCLATURE

ABB Asea Brown Boveri Ltd

AFR (Stoichiometric) Air Fuel Ratio

ATM Atmospheric (Test Rig)

c Concentration

CHP Combined Heat and Power

$CH_4$ Methane

CL Chemiluminescence

CO Carbon Monoxide

$CO_2$ Carbon Dioxide

DLR German Aerospace Center

$\phi$ (Air-Fuel) Equivalence Ratio

$H_2$ (Molecular) Hydrogen

HAB Height Above Burner

IR Infrared

FLOX Flameless Oxidation

$k_1$ Reaction Rate Coefficient

LHV Lower Heating Value

$\dot{m}$ Mass Flow

MGT Micro Gas Turbine

MILD Moderate or Intense Low-oxygen Dilution Combustion

MTT Micro Turbine Technology b.v.

$N_2$ (Molecular) Nitrogen

NO Nitrogen Oxide

$NO_2$ Nitrogen Dioxide

$NO_X$ Nitrogen Oxides

O Atomic Oxygen

OH Hydroxyl Radical

OH* Hydroxyl Radical, Electronically Excited State

p Pressure

$P_{th,n}$ Thermal Power, normalized to Base Load

PLIF Planar Laser-induced Fluorescence

$s_L$ Laminar Flame Speed

T Transmittance

t Time

$T_{ad}$ Adiabatic Flame Temperature

$\tau_{ign}$ Ignition Delay Time

UHC Unburned Hydrocarbons

UV Ultra-violet

## INTRODUCTION

In order to decrease the usage of fossil fuels and nuclear power, the percentage of energy consumption from renewable energies in Germany has more than doubled over the last decade [1]. Since wind and solar power are volatile renewable energy sources, an alternative solution is needed to compensate for fluctuations in energy and to provide demand responsive electricity. A promising contribution is the use of desulfurized biogas from fermentation processes (i. e. plant material, agricultural waste or energy crops). Biogas mainly consists of methane and carbon dioxide ($CO_2$) with a volume fraction of carbon dioxide typically up to 50 %. However, the specific biogas composition depends on the substrate and the operation mode of the digester, therefore the biogas quality is fluctuating. Biogas, as a renewable source, is permanently available, storable and reduces the $CO_2$ footprint of the power generation. Currently, biogas is either used for power generation directly at biogas power plants via combined heat and power (CHP) systems or is

processed to natural gas quality and fed into the public gas grid. However, both options feature energy losses. For example, a considerable part of the waste heat generated by electricity production usually cannot be used as process heat in the biogas plant [2]. Additionally, feeding heat into a district heating grid is often connected with losses, since biogas plants are mainly in a far distance to the users [2]. When biogas is fed to the natural gas grid, however, besides desulfurization and drying, the $CO_2$ must be separated. The $CO_2$ separation is accompanied by high energy demand in terms of power and/or heat. Furthermore, depending on the applied technique, considerable high methane losses occur [2]. Thus, an approach, where the desulfurized biogas is fed into local biogas grids and is used directly for heat and power generation at the end user, is a preferable option. Direct biogas utilization in the grid results in a more efficient use of the fuel. But with this approach, there is a need for fuel flexible CHP systems suitable for end users and with the ability to cope with fluctuating biogas and natural gas qualities, which effectively provide reliable heat and power supply.

CHP systems based on micro gas turbines (MGT) offer advantages over commonly used gas engine based systems, such as the ability to operate without exhaust gas treatment and the need for less maintenance, although the electrical efficiency is currently still lower than for gas engines. With the use of biogas and natural gas as a fuel in the CHP systems, the combustion system of the MGT must accommodate a wide range of fuel compositions and mass flows (due to different heating values). Therefore, FLOX®-based combustors have proven to achieve highly reliable combustion at fluctuating fuel compositions, while producing low exhaust gas emissions [3]. The FLOX® concept itself, originates from industrial furnaces and is based on flameless oxidation, which is also known as volume or MILD combustion [4, 5]. Although, the combustor presented in this paper is usually not operated in the flameless regime, but in a combustion regime with mostly discrete flames, it is characterized by high momentum jets and dilution by flue gas via (internal) recirculation. Therefore, it is referred to as FLOX®-based concept. Here, the fuel is injected coaxially into a high momentum air flow via a fuel nozzle as shown in Fig. 1.

Air and fuel are partially premixed within the mixing section before entering the combustion chamber. The high jet velocity reduces the risk for flashbacks even with pure hydrogen significantly

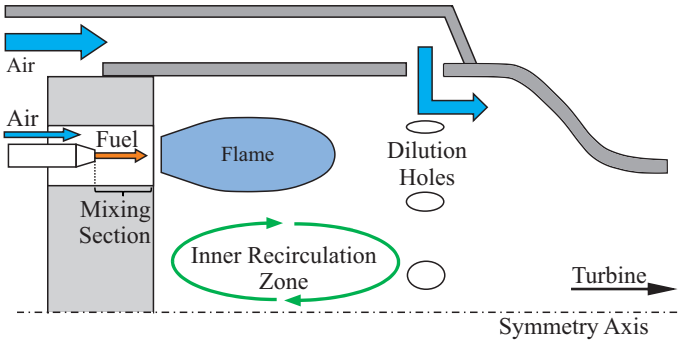


Fig. 1: Schematic of FLOX®-based Combustion Principle

[6] and promotes, in combination with the surrounding geometry, a strong inner recirculation zone. This recirculation dilutes the incoming fresh gas with hot exhaust gas and leads to a homogeneous temperature distribution without local temperature peaks which is essential for low $NO_x$ emissions [4, 5]. In a MGT only a part of the global air mass flow takes part in the combustion as primary air. The major part of the air is guided alongside the liner and enters the combustion chamber typically via dilution holes in order to reduce the exhaust gas temperature before entering the turbine (see Fig. 1). Furthermore, a part of the secondary air can be used as cooling air for the surrounding structures (not shown in Fig. 1).

For the use in MGTs, two FLOX®-based combustion systems have been developed and tested in an Ansaldo "AET100" MGT (former known as Turbec "T100") with an electrical power output of 100 kW. Whereas Zornek et al. [7–9] developed a ten nozzle combustor for the use with low calorific fuel from wood gasification, Zanger et al. [10, 11] developed one for the application of natural gas with 20 nozzles. Both systems are equipped with a FLOX®-based main stage and a swirl-based pilot stage. The ten nozzle combustor was studied in terms of its fuel flexibility by Bower et al. [12] at atmospheric pressure with regard to combustion stability and emissions. They varied the lower heating value from 7 – 49 MJ/kg by applying syngas (32 vol.-% $H_2$, 32 vol.-% CO, 18 vol.-% $CO_2$, 18 vol.-% $N_2$), methane and a mixture of both, respectively, at air preheat temperatures of 873 K. Furthermore, different thermal loads and equivalence ratios were investigated. At constant equivalence ratio, a consistent flame shape for all tested lower heating values and thermal powers was observed. Moreover, Zornek et al. [3] studied the influence of the hydrogen content in the syngas (0 % to 30 %) on emissions and flame characteristics of the combustor in a

Turbec T100 test rig. OH PLIF measurements depicted a strong influence of the hydrogen content on the OH radical distribution. Though, $NO_X$, CO and UHC emissions remained consistent below 10 ppm (at 15 vol.-% residual oxygen), except for the CO emissions in the case without any hydrogen in the syngas. The two-staged combustion system could be operated stably in all tested conditions.

The combustion system presented in this paper was developed for the application in a MGT with an electrical power output of 3 kW. It is characterized by six air/fuel nozzles and only one combustion stage. It was studied in detail with natural gas as the fuel under atmospheric conditions regarding the influence of preheat temperature, thermal power and equivalence ratio on emissions, flame shape and location and stable operating range [13]. The combustor could be operated stably with $NO_x$ emissions below 15 ppm and CO emissions below 25 ppm (both at 15 vol.-% residual $O_2$) for all MGT relevant load points. This paper experimentally evaluates the impact of biogas on this six-nozzle FLOX®-based combustor. In this study, three different fuel compositions are used: natural gas and two mixtures of natural gas with $CO_2$, containing 25 % (biogas 1) and 50 % (biogas 2) by volume $CO_2$, respectively. Unlike biogas, natural gas contains higher hydrocarbons. The influence on the combustion of the addition of upto 20 vol.-% ethane to methane was investigated in [14]. It was shown, that an increase in ethane leads to more discrete flames, lower CO emissions at low equivalence ratios and a shift of lean blow out to leaner combustion conditions. Though, the sensitivity to ethane addition increases with approaching lean blow out conditions. In the investigations presented in this paper, only slight influences of higher hydrocarbons in the fuel are expected. On the one hand, the fraction of higher hydrocarbons within the natural gas was rather low with $\leq$4.7 vol.-%, on the other hand it is expected that the investigated load points are not close to the lean blow out limit [13].

The combustor was first tested at atmospheric conditions in an optical accessible test rig, without dilution and cooling air. The influence of $CO_2$ admixture on $NO_x$ and CO emissions was investigated at thermal powers corresponding to the MGT part and base loads and varying equivalence ratios. The shape and position of the flame was visualized using OH*-chemiluminescence (OH* CL). Based on the atmospheric test results, the combustion system design for the integration

Table 1: Fuel mixtures

| | $X_{NG}$ | $X_{CO2}$ | LHV | $AFR_{st}$ |
|---|---|---|---|---|
| | vol.-% | vol.-% | MJ/kg | kg/kg |
| Natural Gas | 100 | 0 | 47.3...47.7 | 16.3...16.4 |
| Biogas 1 | 75 | 25 | 24.7...25.6 | 8.5...8.8 |
| Biogas 2 | 50 | 50 | 12.6...13.3 | 4.4...4.6 |

into the MGT was derived (especially the desired split between primary and secondary air) and implemented into a prototype micro gas turbine CHP system (”EnerTwin” of Micro Turbine Technology b.v.). In the MGT, the influence of $CO_2$ addition (biogas 1 and 2) was analyzed from part to base load and compared to natural gas.

## EXPERIMENTAL SETUP

The fuel flexibility of this combustor was tested using the three different fuel compositions, which are shown in Tab. 1.

For all measurements, natural gas with a typical composition of $CH_4$ = 93.1 - 93.9 vol.-%, $C_{2+}$ = 4.2 - 4.7 vol.-% and inert species = 1.9 - 2.2 vol.-% was used either as ”pure” natural gas or in a mixture with $CO_2$.

Within this paper, the burner equivalence ratio is given as

$$\phi = \frac{\text{air mass flow for stoichiometric conditions}}{\text{actual air mass flow}}. \tag{1}$$

A flue gas sample is continuously taken from the exhaust gas duct and sampled with a rate of 1 Hz. At the atmospheric test rig, the probe is air cooled coaxially to a tip temperature of less than 405 K to guarantee a sufficient quenching of the chemical reactions as well as suppressing surface reactions of CO at hot probe walls. The exhaust gas probe temperature is monitored to prevent

Table 2: Ranges and corresponding accuracies of measured exhaust gas species

| Analyzed Species | $NO_x$ ppm | CO ppm | UHC $mgC/m^3$ | $O_2$ vol.-% | $CO_2$ vol.-% |
|---|---|---|---|---|---|
| Range 1 | 0 - 10 | 0 - 10 | 0 - 10 | 5 - 15 | 0 - 5 |
| Accuracy 1 | 0.1 | 0.1 | 0.2 | 0.075 | 0.05 |
| Range 2 | 10 - 20 | 10 - 100 | | 15 - 25 | 5 - 20 |
| Accuracy 2 | 0.2 | 1.0 | | 0.125 | 0.2 |
| Range 3 | 20 - 50 | | | | |
| Accuracy 3 | 0.5 | | | | |

condensing of the water. NO and $NO_2$ are detected via an UV photometer (ABB “Limas11”) from the wet exhaust, whereas CO and $CO_2$ are measured from the dry exhaust gas using an IR photometer (ABB “Uras26”). The unburned hydrocarbons (UHC) are identified by means of a flame ionization detector (ABB “MultiFID14”). The residual oxygen concentration of the dry flue gas was measured using an analyzer based on paramagnetism (ABB ”Magnos206”), whereas the water concentration was detected capacitively (Vaisala “HMT338”). The accuracies of the individual analyzers are given in Tab. 2. All results are time averaged over at least 5 min and normalized to dry conditions at a residual oxygen content of 15 vol.-%.

**Atmospheric Test Rig**

*Setup of Test Rig.*

The experimental analysis of the combustor was performed in an atmospheric test rig with an optically accessible cylindrical combustion chamber as shown in Fig. 2. This allows the application of optical measurement techniques like OH*-chemiluminescence. Furthermore, the test rig offers the possibility to test the combustor without the limitations of the MGT operating conditions. The air was electrically preheated to 730 °C which corresponds to the MGT combustion chamber inlet temperature. The spark plug in the lower section of the combustion chamber is only used for igniting the air/fuel mixture. In order to ensure similar flow fields (and therefore similar pressure loss, flow velocities and residence times) as in the MGT application, the pressure difference

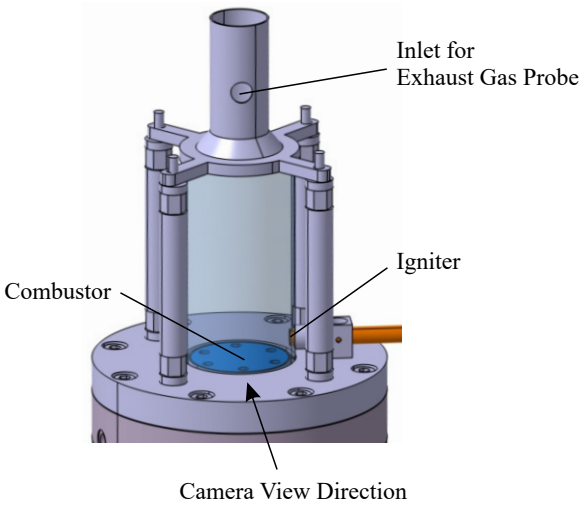


Fig. 2: Experimental Setup of Atmospheric Test Rig

between the MGT and the atmospheric test rig was taken into account by applying mach number similarity. Since a scaling of the geometry is not reasonable due to the already small dimensions of the combustor, the mass flows were chosen as the scaling parameter. Assuming constant heat capacity ratio and with similar fluids, geometry and combustion chamber inlet temperatures, the mach number similarity results in the scaling equation

$$\dot{m}_{ATM} = \dot{m}_{MGT} \cdot \frac{p_{ATM}}{p_{MGT}}. \tag{2}$$

The boundary conditions for the atmospheric tests (as well as for the MGT tests) are shown in Tab. 3. The thermal power is normalized with respect to MGT base load and scaled according to Eq. 2 for the atmospheric tests. The combustor chamber inlet pressure varies from 1.86 to 2.8 bar within the operating range of the MGT. Therefore, the normalized thermal power of minimum part load is $P_{th,n}$ = 46.5 % for the MGT test case and $P_{th,n}$ = 69 % for the atmospheric tests. Since the combustion chamber inlet temperature $T_{cc,in}$ is almost constant for part and base load of the MGT, it was fixed to 730 ℃ was for the atmospheric tests. As it is not possible to measure the split between primary and secondary air in the MGT, the equivalence ratio at the combustor is only given for the atmospheric setup. Within the atmospheric tests, the equivalence ratio $\phi$ was

Table 3: Test Conditions

| Parameter | Range | | Unit |
|---|---|---|---|
| | ATM | MGT | |
| $P_{th,in,n}$ | 69 & 100 | 46.5 - 100 | % |
| $T_{cc,in}$ | 730 | 725 - 734 | °C |
| $p_{cc,in}$ | 0.98 - 1.01 | 1.86 - 2.80 | bar |
| $\phi$ | 0.28 - 0.56 | - | - |

varied between 0.28 and 0.56. Since the combustion chamber inlet temperature $T_{cc,in}$ is almost constant between part and base load of the MGT, only 730 °C was applied in the atmospheric tests. In contrast to the combustion chamber inlet temperature, the combustion chamber inlet pressure varies from 1.86 to 2.8 bar within the operating range of the MGT. Since it is not possible to measure the split between primary and secondary air in the MGT, the equivalence ratio at the combustor is only given for the atmospheric setup. Within the atmospheric tests, the equivalence ratio $\phi$ was varied between 0.28 and 0.56.

*Instrumentation.*

The test rig was equipped with detailed instrumentation to analyze all relevant parameters. The data acquisition was carried out with “Delphin” modules with an output frequency of 2 Hz. The combustor inlet temperature was measured using the arithmetic average of two thermocouples (Type N, tolerance class 1) close to the nozzle inlet. At a preheat temperature of 730 °C the measurement uncertainty is $\pm$ 2.9 K. The air mass flow was controlled by a “Bronkhorst EI-Flow F-203” with a measurement uncertainty of $<$ 1.80 %, whereas for the natural gas mass flow a “Bronkhorst Mini-Cori-Flow M14” with a measurement error of $<$ 2.01 % and for the carbon dioxide a “Bronkhorst F-113” with an uncertainty of $<$ 3.8 % were used. The flue gas was probed in the exhaust gas duct as shown in Fig. 2.

*OH*-Chemiluminescence.*

The shape and location of the heat release zone was visualized using OH*-chemiluminescence. Since OH* is formed in the heat release zone and has a very short life time, its emitted chemiluminescence signal is a reasonable indicator for the heat release zone [15, 16]. The OH* CL signal was imaged with an intensified CCD camera (LaVision "Imager Pro Plus 2M"), which was equipped with an UV lens and a high-transmission bandpass filter (Laser Components GmbH, $T > 80\,\%$ at 310 nm). Furthermore, color glass filters (Schott, "UG11") were used to block the background luminescence of the metal parts of the combustion chamber. At each operating point at least 600 statistically independent images were recorded with a constant gain. Due to a considerable difference in OH* CL signal intensity between the studied operating points, exposure times between 25 and 450 $\mu$s were applied. During post processing the images were corrected for background and camera sensitivity and time averaged. Furthermore, each image was scaled to its maximum intensity. Since OH* CL is a line-of-sight method, the signal is spatially integrated through the combustion chamber. There are six nozzles in the camera field of view, with three in the front and three in the back. Since the front nozzles are in-line with the back nozzles, only three flame regions are depicted in the analyzed images. Figure 3 shows a horizontal section through the combustion chamber with the field of view of the OH* CL camera.

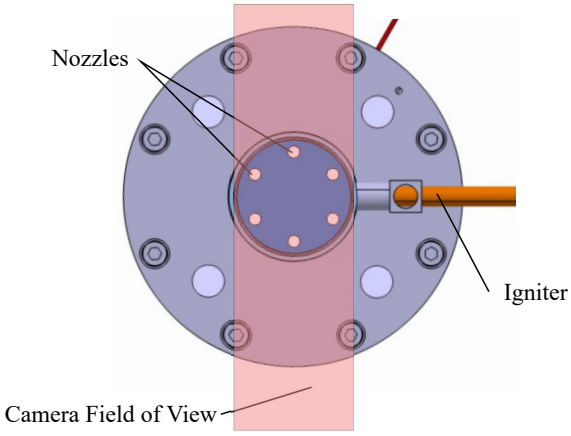


Fig. 3: Horizontal Section Through the Combustion Chamber at the Atmospheric Test Rig

**Micro Gas Turbine Test Rig**

*Micro Gas Turbine.*

The combustion system was tested in an MTT ”EnerTwin” CHP system. The system has an electrical power output of 3 kW and a thermal power output of up-to 14.4 kW with a pressure ratio of 3. A scheme of the MGT cycle and the relevant instrumentation is shown in Fig. 5. At first, ambient air is compressed by the compressor (1) up to approximately 3 bars. Before entering the combustor (3), the air is pre-heated with hot exhaust gas in the recuperator (2). In the combustor, the fuel is injected and oxidized and the hot exhaust gas is expanded through the turbine (4) and heats the compressed incoming fresh air in the recuperator (2). In the subsequent water heat exchanger (5) the thermal power (e.g. for use in a heating system) is coupled out. Compressor (1), turbine (4) and generator (7) are mounted on the same shaft (6). In contrast to the atmospheric test rig, the combustor is operated with dilution air in the MGT. Therefore, the secondary air guidance for the natural gas combustion system was at first designed using CFD, based on the successful tests of the natural gas combustor at atmospheric pressure published in [13]. A burner equivalence ratio of $\phi$ = 0.48 at base load (corresponding to an equivalence ratio of approximately 0.36 at part load) was found to be the best compromise between emissions (CO and $NO_x$) and total pressure loss. When designing the combustion system for the MGT application, especially the location and the geometric opening area of the dilution holes have to be defined. Since the split between primary and dilution air can be adjusted by varying the opening area of the dilution holes, their diameter was iteratively adapted using CFD simulations, until the desired air split was reached. The resulting prototype was integrated into the MGT based CHP system ”EnerTwin” and studied using natural gas especially with regard to its emitted exhaust gas emissions and its combustion stability. The experimental investigations of the combustion system in the MGT were carried out using two different versions of the ”EnerTwin” CHP system. While the combustion system was adjusted for the use with biogas and tested under atmospheric conditions, the ”EnerTwin” CHP system was developed further by the manufacturer. Therefore, it was decided to perform the biogas tests with the latest system in order to use a more advanced system which is closer to the market. Concerning the combustion system, the main difference between the two CHP systems is a modification of the

secondary air flow path at the transition to the turbine. For the integration of the combustion system into the enhanced ”EnerTwin” version, a few design modifications concerning the secondary air guidance had to be made. Furthermore, compared to the first MGT experiments with natural gas the liner design was optimized with regard to thermal stresses. The two different configurations can be seen in Fig. 4. The narrowest cross sections of all open surfaces of the secondary

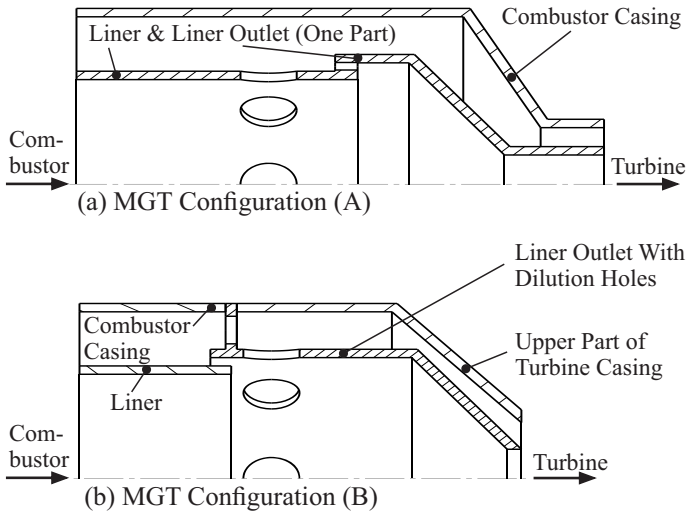


Fig. 4: Schematic of MGT Secondary Air Flow Path Design for Configuration (A) and (B)

air flow path (dilution holes, cooling gaps) were held constant, since a change in pressure loss within the secondary air path will directly influence the split between primary and secondary air flow and therefore will change the local combustion conditions at the burner. The combustion system, which has been adapted in terms of fuel application and secondary air flow guidance, was integrated into the MGT and tested with natural gas, biogas 1 and biogas 2. In the further course of this paper, the combustion system for the advanced ”EnerTwin” version is referred to as combustion system (B), whereas the one for the preceding version is referred to as combustion system (A).

*Instrumentation.*

The MGT was equipped with detailed instrumentation. The instrumentation, relevant for this paper, is shown in Fig. 5.

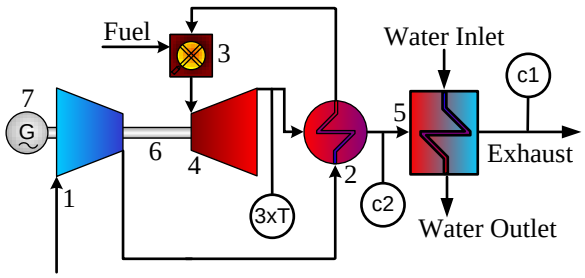


1 Compressor
2 Recuperator
3 Combustor
4 Turbine
5 Water Heat Exchanger
6 Shaft
7 Generator

T Thermocouple (Turbine Outlet)
c1 Exhaust Gas Probe Position 1
c2 Exhaust Gas Probe Position 2

Fig. 5: Scheme of MGT Cycle and Instrumentation

The turbine outlet temperature is determined by the arithmetic average of three thermocouples (type K, tolerance class 2) with a measurement uncertainty of $\pm$ 5.9 K. All other thermocouples were type N with tolerance class 1 and a resulting uncertainty of $\pm$ 2.9 K. In the first campaign with combustion system (A), the exhaust gas probe was taken after the recuperator (c2), since a control of the water temperature was not possible, here. Hence, at (c1) it could not be guaranteed that no water would condense from the exhaust gas. In the subsequently following campaign with combustion system (B), the MGT test rig was improved, so that the water temperature could be controlled and the exhaust gas could be extracted from the exhaust gas duct after the water heat exchanger (c1). The inlet temperature of the water into the water heat exchanger (5) was controlled to temperatures above 320 K in order to prevent water condensing from the exhaust gas. Due to the rather low exhaust gas temperature at (c2), different results between the two measurement locations are not expected. Since the focus for this study is the combustion system and its emissions, the automatic control system of the MGT was not adapted for the use of other fuels than natural gas at this point. Instead, the MGT was controlled manually to a constant turbine outlet temperature of 1060 K by adjusting the fuel mass flow.

## RESULTS AND DISCUSSION

### Combustor Operated in the Atmospheric Test Rig

Previous work has shown that the combustor can be stably operated with natural gas over a wide operating range with a total pressure loss $\leq$1.5 % [13]. Since the pressure loss is mainly determined by the air mass flow and not by the fuel, the focus of this paper is on the influence of the fuel gas composition on the emissions and the heat release zone. Compared to the former experiments, the outlet diameter of the fuel nozzles has been increased to account for the almost doubled fuel volume flow when using biogas 2, in order to reduce the pressure loss over the fuel nozzles. Therefore, the fuel/air-velocity ratio for natural gas as fuel changes. An experimental study of this combustor has shown that the resulting change in CO and $NO_x$ emissions lies within the measurement accuracy of other boundary conditions, e. g. thermal power or equivalence ratio [17]. Due to the geometry of the nozzles and the mixing section, the large scale turbulence seems to be dominant compared to the small scale turbulence resulting from the velocity ratio of fuel and air, here. Besides stable combustion and pressure loss, the $NO_x$ and CO emissions limit the later operating range of the combustor. In Germany, the exhaust gas emissions are limited for gas turbines in this power class to 75 mg/m$^3$ $NO_x$ at 15 vol.-% $O_2$ ($\approx$ 37 ppm) and 0.10 g/m$^3$ CO at 15 vol.-% $O_2$ ($\approx$ 80 ppm) during operation with a load of $\geq$70 percent [18].

*Emissions.*

Figure 6 shows the dry $NO_x$ emissions for the investigated operating range of $0.278 < \phi < 0.56$ for thermal powers corresponding to part and base load and with natural gas and the two biogas mixtures (see Tab. 1) as fuel. As can be seen, for all studied conditions, the $NO_x$ emissions are far below the legal limit of 37 ppm.

Due to the exponential temperature dependency of the thermal $NO_x$ formation, the $NO_x$ emissions increase with increasing equivalence ratio and therefore increasing combustion temperature. As presented before [13], the $NO_x$ emissions of this combustor are not very sensitive to the applied changes in thermal power and thus the applied changes in residence time, especially at leaner conditions. The combustion rate of thermal $NO_x$ becomes rather low for combustion temperatures below 1850 K [19]. For adiabatic conditions, the combustion temperature, with natural gas as the

fuel, drops below this limit for equivalence ratios $\phi \lesssim 0.38$. Since the combustion chamber at the atmospheric test rig is not insulated, it can be expected that this temperature limit is reached at an even higher equivalence ratio. As the (thermal) $NO_x$ emissions are overall at a low level and the formation rate is rather low, the $NO_x$ emissions are not sensitive to an increase in residence time within the studied operation range. Thus, there is no significant dependency of the $NO_x$ emissions from the thermal power. The addition of $CO_2$ to the fuel lowers the $NO_x$ emissions for a constant equivalence ratio. Here, different effects superimpose. First of all, for a given equivalence ratio, the adiabatic flame temperature decreases with increasing $CO_2$ fraction of the fuel. Furthermore, the $O_2$ (and $N_2$) concentration of the total mixture decreases and therefore, the formation rate is reduced according to

$$\frac{c_{NO}}{dt} = 2 \cdot k_1 \cdot c_O \cdot c_{N_2}, \tag{3}$$

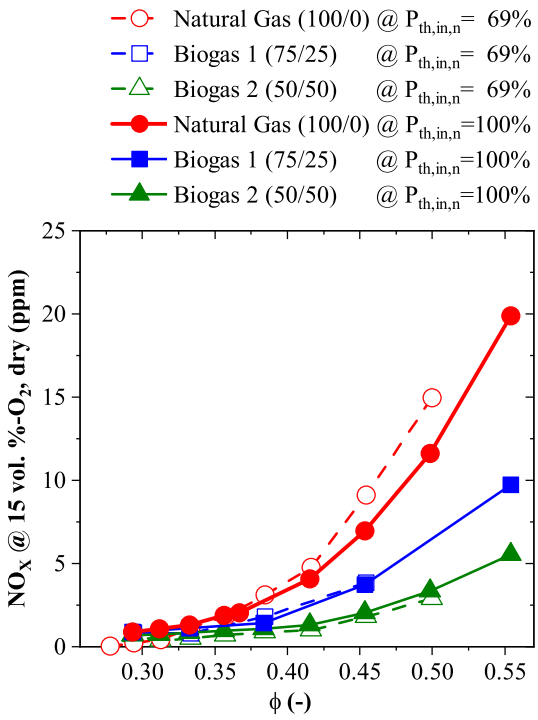


Fig. 6: $NO_x$ Emissions as a Function of Burner Equivalence Ratio $\phi$

With $k_1$ = 1.8·10$^{14}$ exp{(-318 kJ/mol) / (RT)} cm$^3$/(mol s) [20, 21]. Hence, the amount of $NO_x$ emissions is reduced for constant residence time. Since the mean residence time changes only about 1.1 % in maximum between natural gas and biogas 2, it can be seen constant. Due to the admixture of $CO_2$ the flame temperature is decreased, which leads to a decrease in $NO_x$ emissions. Thus, non-perfectly premixed regions produce less $NO_x$ than in the case without $CO_2$ addition [21]. The $NO_x$ reducing effect of $CO_2$ addition can be seen in Fig. 6 especially at high equivalence ratios and higher adiabatic flame temperatures, respectively. This was also observed for a swirl combustor by Burdet et al. [22].

The CO emissions of the combustor are shown in Fig. 7 as a function of the burner equivalence ratio at part and base load for the three fuels. For high equivalence ratios, the CO emissions

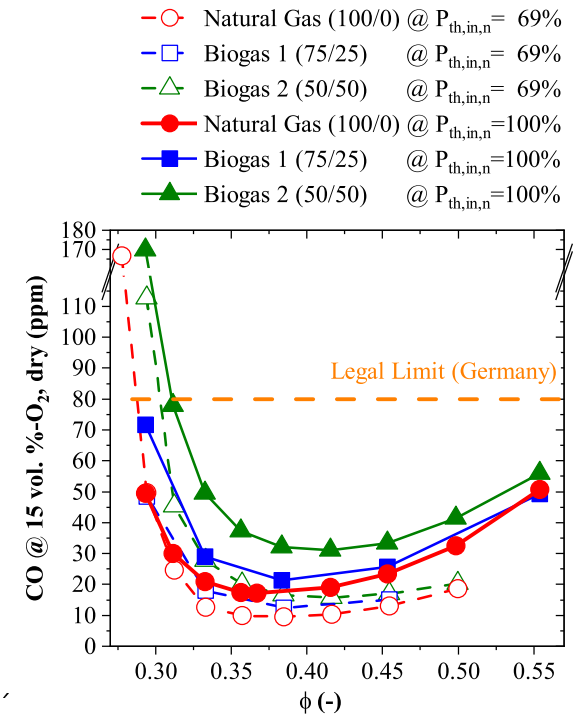


Fig. 7: CO Emissions as a Function of Burner Equivalence Ratio $\phi$

follow the trend of the chemical equilibrium and decrease with decreasing equivalence ratio (and increasing oxygen content, respectively) until they reach a minimum at equivalence ratios between $\phi \approx$ 0.39 - 0.42. For a further decrease in equivalence ratio, the CO emissions rise significantly

due to non-equilibrium effects. On the left hand branch of the CO emission profile in Fig. 7, two effects superimpose. On the one hand, the reduction in combustion temperature slows down the chemical reactions and on the other hand, the mean residence time decreases with decreasing equivalence ratio, here. Since the thermal power is kept constant, the air mass flow, and hence the volume flow, increases with decreasing equivalence ratio. Assuming an exhaust gas temperature corresponding to the adiabatic flame temperature, the volume flow, e.g. for biogas 2, increases on the left hand branch by approximately 23 % between $\phi = 0.42$ and $\phi = 0.29$ and therefore, the average residence time decreases, respectively. With decreasing equivalence ratio the reaction rates for the CO oxidation become too slow for the corresponding residence time and lead to a rise in CO emissions.

In contrast to the $NO_x$ emissions, the CO emissions are not independent of the thermal power as already shown in [10, 13]. At constant equivalence ratio (and constant fuel mixture) and therefore constant adiabatic flame temperature, the average residence time decreases due to the higher volume flow at elevated thermal power in the range of approximately 44 – 60 % between $\phi = 0.5 - 0.28$. This leads to a rise of CO emissions with increasing thermal power. The addition of $CO_2$ to the fuel shifts the CO emission profile to a higher level and the minimum of the profile to higher equivalence ratios. The higher level of the profile might be caused by the increased $CO_2$ concentration, which shifts the chemical equilibrium towards CO leading to higher CO emissions. Since the adiabatic flame temperature is lower at constant equivalence ratio with increasing $CO_2$ concentration, the rise in CO emissions at decreased equivalence ratios occurs already at higher equivalence ratios triggered by the non-equilibrium effects.

The measured emissions of unburned hydrocarbons were below the detection threshold of the analyzer.

*Flame Shape and Location.*

The flame shape and location was determined using OH* chemiluminescence. Figure 8 shows two series (natural gas and biogas 2) of time-averaged OH* CL images at a constant normalized thermal power of $P_{th,n}$=100 % at a preheat temperature of 730 °C.

Within each series the equivalence ratio was varied from $\phi = 0.56$ to $\phi = 0.29$. The respective

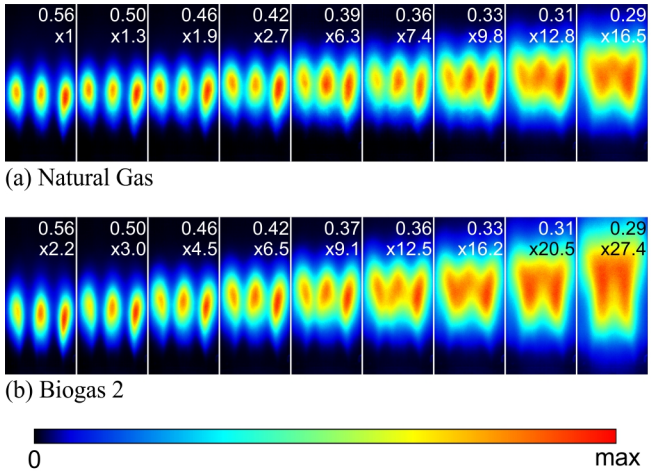


Fig. 8: Time Averaged OH* CL Images at $P_{th,n}$ = 100 % for the Variation of $\phi = 0.29 - 0.56$ for Natural Gas and Biogas 2

equivalence ratio is displayed in the upper right corner of each image. Since each image is normalized to its maximum, the respective intensity scaling factor is given as well. It ranges from 1 at $\phi$ = 0.56 with natural gas (s. Fig. 8a) to 27.4 at $\phi$ = 0.29 with biogas 2 (s. Fig. 8b). With decreasing equivalence ratio, the flame shape changes from discrete single flames to a more distributed flame regime. In order to quantify the changes in flame shape and location, two parameters are introduced: the height above burner (HAB) and the dispersion of the OH* CL signal. Here, only signals above 50 % of the maximum intensity are taken into account. The HAB is the axial distance (normalized to the nozzle diameter) from the nozzle outlet to the averaged horizontal boundary of the flames. The dispersion is the ratio of the flame area, determined with the OH* CL signal, and the field of view. It serves as a measure for the distribution of the combustion and is also shown in Fig. 9. With increasing equivalence ratio the combustion becomes more distributed as indicated by the rising dispersion of the OH* CL signal. For higher equivalence ratios there is almost no difference between natural gas and biogas 2. However, with decreasing equivalence ratio the influence of the $CO_2$ addition increases and the $CO_2$ addition leads to a significantly more distributed flame regime. The (normalized) height above burner $HAB_n$ rises, especially for biogas 2, with decreasing equivalence ratio before decreasing again as the heat release zone becomes more distributed. With biogas 2 as the fuel the combustion shows largely a lower (normalized) HAB

as for natural gas. The data points at $\phi \approx 0.38$ (biogas 2) and $\phi \approx 0.36$ (natural gas) are artifacts of the post processing algorithm. In this equivalence ratio range discrete flames merge to more homogeneous reaction zones. Compared to natural gas, the heat release zone is largely more

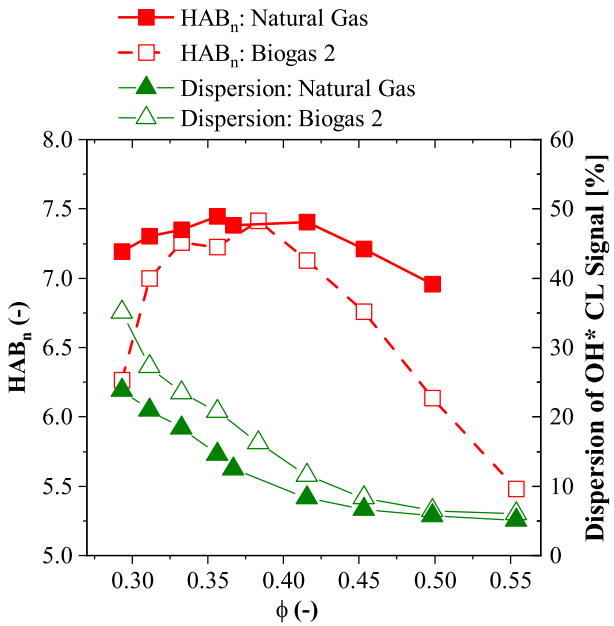


Fig. 9: Normalized Height Above Burner and Dispersion for Natural Gas and Biogas 2 as a Function of Burner Equivalence Ratio $\phi$

distributed for biogas with a lower HAB at constant equivalence ratio. Assuming no difference in terms of turbulence between natural gas and biogas, the more distributed combustion has to result from changes in chemical kinetics. Unfortunately, there are no information about the local species, temperature and velocity distribution in the combustion chamber available. Therefore, only global conditions can be considered, here. Figure 10 shows the relative difference in laminar flame speed $s_L$, ignition delay time $\tau_{ign}$ and adiabatic flame temperature $T_{ad}$ between natural gas and biogas 2 (with respect to natural gas) as a function of the burner equivalence ratio $\phi$. The laminar flame speed $s_L$ was determined using Cantera with diffusion properties calculated from a multi component diffusion model including thermodiffusion. The ignition delay time $\tau_{ign}$ was calculated using Chemical Workbench with a homogeneous reactor with adiabatic boundary conditions at constant pressure. As the ignition criterion the maximum temperature gradient was selected. The adiabatic

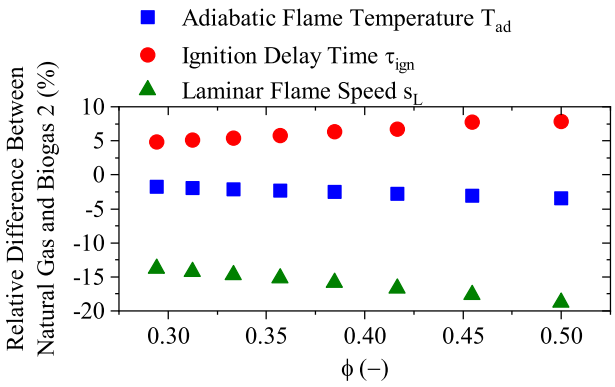


Fig. 10: Relative Difference of Laminar Flame Speed $s_L$, Ignition Delay Time $\tau_{ign}$ and Adiabatic Flame Temperature $T_{ad}$ Between Natural Gas and Biogas 2 as a Function of Burner Equivalence Ratio $\phi$ at 1 bar and an Air Preheat temperature of 730 °C

flame temperature is calculated assuming constant enthalpy and isobaric conditions. As reaction mechanism, the C1 - C3 mechanism (version 1911) [23–25], which includes 114 species and 1999 reactions, was used. While the ignition delay time at combustor inlet conditions increases only by 4.7 to 7.8 % (depending on the equivalence ratio) between natural gas and biogas 2, the laminar flame speed decreases significantly by 13.8 to 18.7 % (depending on the equivalence ratio). Additionally, at constant equivalence ratio, the adiabatic flame temperature is reduced by 29 to 68 K (depending on the equivalence ratio) between biogas 2 and natural gas. Therefore, the temperature of the recirculated exhaust gas is lower. Altogether, this leads to a more distributed flame for biogas 2 than for natural gas at constant burner equivalence ratio. Though, the differences in ignition delay time and adiabatic flame temperature become smaller with decreasing equivalence ratio, the influence on the heat release distribution becomes more significant. In contrast to the swirl-combustor presented in [22], the heat release zone is shifted upstream when $CO_2$ is added to the incoming gas mixture. For the later operation of the combustion system in the MGT, the lower adiabatic flame temperature with biogas at constant equivalence ratio has to be compensated by increasing the equivalence ratio about $\Delta\phi \approx 0.04$ in order to reach similar turbine outlet temperatures. The slight asymmetries occurring in Fig. 8 most likely result from manufacturing tolerances and the slight asymmetry of the combustion chamber caused by the igniter as shown in Fig. 2.

**Combustor Operated in the Micro Gas Turbine Based CHP System "EnerTwin"**

As described before, at first, an "EnerTwin" was operated with the FLOX®-based combustion system (A) and natural gas. The combustion system could be operated stably in all load points of the MGT. Figure 7 depicts its CO and $NO_x$ emissions as a function of turbine speed. A turbine speed of 240 krpm corresponds to base load and 180 krpm to part load. The dry CO and $NO_x$ emissions are normalized to 15 vol.-% residual oxygen content. As can be seen, the $NO_x$ emissions are in the single-digit range and therefore, far below the legal limit of 37 ppm. For high turbine speeds, and thus high equivalence ratios and high combustion temperatures, they show a slight rise. Compared to the emissions published in [26] for the original combustion system, the $NO_x$ emissions could be reduced by the FLOX®-based combustor by more than one magnitude.

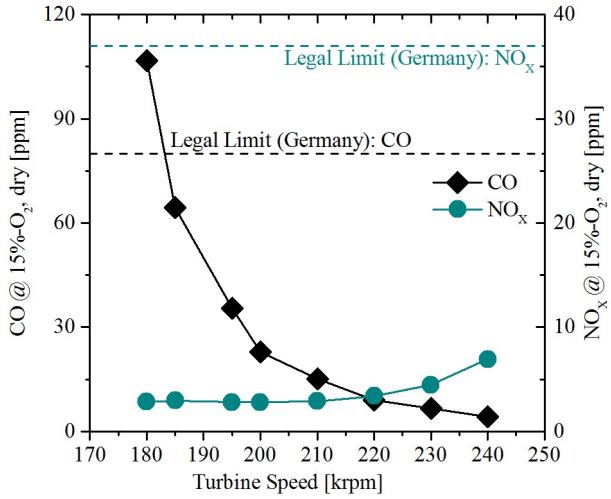


Fig. 11: CO and $NO_x$ Emissions of the "EnerTwin" operated with the FLOX®-based Combustion System (A) and Natural Gas

The CO emissions rise with decreasing turbine speed from approximately 5 ppm at base load to little more than 100 ppm at part load. Since the burner equivalence ratio decreases, and therefore the combustion temperature decreases as well with decreasing turbine speed, the combustor operates on the left hand branch of the CO emission profile shown in Fig. 7. Since the emissions are only regulated for loads of $\geq$70 %, what corresponds to turbine speeds above approximately 217.000 rpm, the CO emissions, as well as the $NO_x$ emissions, are far below the legal limits. The

value of 80 ppm is just exceeded right before reaching the part load operating point.

The fuel flexibility of the combustor and the influence of biogas on the combustion were studied using the advanced ”EnerTwin” version with combustion system (B). It could be operated stably in the complete stationary operating range of the MGT from part to base load.

The CO emissions of the combustion system (B) are shown in Fig. 12 for the three different fuel mixtures (s. Tab. 1). As expected, the CO emissions rise with increasing $CO_2$ concentration of the

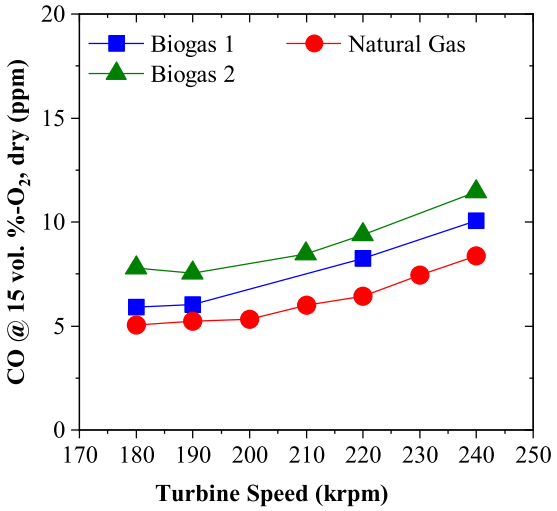


Fig. 12: CO Emissions of the advanced ”EnerTwin” operated with the FLOX®-based Combustion System (B) and Different Fuels

fuel. All in all, the CO emissions are on a very low level for all three studied fuels in the complete stationary operating range of the MGT. Especially at lower turbine speeds, the CO emissions are significantly lower than with the combustion system (A) (see Fig. 11) and are below the legal limit of 80 ppm in the complete stationary operating range of the MGT. Furthermore, in contrast to combustion system (A), the CO emissions of the combustion system (B) decrease with decreasing turbine speed. This indicates that the combustion system (B) operates on the right hand branch of the CO emission profile shown in Fig. 7. Although, the open surfaces of the dilution holes and cooling air gaps were held constant between systems (A) and (B), the equivalence ratio at the combustor seems to be shifted to higher values, which means a larger part of the global air flow is guided through the secondary air path. Since the distribution of the air depends on the

pressure loss ratios across the various openings, the pressure loss ratios between the combustor nozzles, dilution holes and the different cooling air gaps must have changed. Most likely the difference results from changes in pressure loss due to geometry modifications or additionally from resulting impacts of the surrounding system. Since the MGT is controlled to a constant turbine outlet temperature throughout the range of operation, it is possible that the MGT operates in a slightly different operation point, if the temperature profile at the turbine outlet temperature sensors has changed due to the geometry and air split modifications.

The shift in burner equivalence ratio is also reflected in the $NO_x$ emissions of combustion system (B), which are depicted in Fig. 13. Whereas combustion system (A) has $NO_x$ emissions in

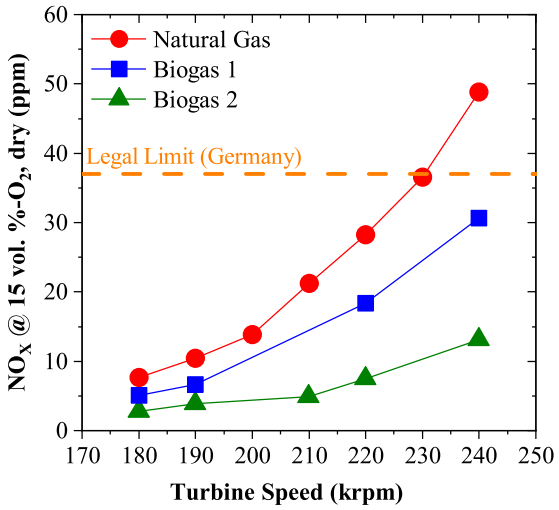


Fig. 13: $NO_x$ Emissions of the advanced "EnerTwin" operated with the FLOX®-based Combustion System (B) and Different Fuels

the single-digit range and the $NO_x$ emission increase at base load conditions is almost negligible, all fuels at combustion system (B) show a considerable rise when approaching base load conditions. Both biogases meet the legal requirements. Though, the limit is exceeded with natural gas for turbine speeds of more than 230.000 rpm. Since the thermal $NO_x$ production is exponentially depended on the combustion temperature [27], a moderate temperature reduction, would be sufficient to reduce the $NO_x$ emissions at base load for meeting the legal requirements. Conse-

quently, the ratio of primary air to secondary air has to be increased only slightly. Based on the atmospheric results a shift in burner equivalence ratio of approximately $\Delta\phi \approx 0.05$ is expected to be necessary to reduce the $NO_x$ emissions from approx. 48 ppm to 37 ppm. But since the CO emissions are extremely low with a large distance to the legal limit, the air split could be shifted significantly towards leaner conditions, which results in a further decrease in $NO_x$ emissions and allows a very good trade-off between $NO_x$ and CO emissions for all tested fuels with combustion system (B). The measured emissions of unburned hydrocarbons are within the accuracy of the analyzer and are therefore negligible.

## SUMMARY

An experimental investigation of the fuel flexibility of a single-staged six nozzle FLOX®-based combustor has been carried out. The study investigated the influence of biogas (natural gas with up to 50 vol.-% $CO_2$) on the stability, the emissions and the flame shape and location. The combustor was studied at atmospheric conditions, as well as in a 3 $kW_{el}$ micro gas turbine CHP system. The combustor could be stably operated in all stationary load points with natural gas, as well as with admixtures of up to 50 vol.-% $CO_2$. The combustor, investigated in this study, is the first single staged FLOX®-based combustor operated successfully in a MGT. Furthermore, it is highly fuel flexible. It was tested in the MGT in two configurations, which differed in the pathway of the secondary air guidance. The first configuration (A) was tested only with natural gas. Configuration (B) was studied in an advanced version of the ”EnerTwin” CHP system with natural gas and biogas. For configuration (B), design modifications concerning the secondary flow path were necessary to integrate the combustion system into the advanced MGT version. However, the secondary flow path is not yet optimized. The $NO_x$ and CO emissions of configuration (A), tested with natural gas, were far below the German legal limit, with $NO_x$ emissions in the single-digit range. Configuration (B) proved its fuel flexibility with natural gas and biogas. Whereas an increase in $CO_2$ content of the fuel resulted in slightly higher levels of the CO emission profiles, the level of the $NO_x$ emissions is reduced. Especially at high adiabatic flame temperatures, the reduction in $NO_x$ due to the $CO_2$ admixture becomes significant. Whereas the CO emissions of configuration (B) were

far below the legal limit in the complete stationary operating range for all three fuel mixtures, the $NO_x$ limit is exceeded for natural gas.

On the basis of the comparison with the atmospheric measurements and the results from the experiments with system (A), it can be deduced that a slight adjustment of the air split to leaner conditions at the combustor, will reduce the combustion temperature and therefore, the $NO_x$ emissions. Based on the atmospheric tests, a split modification resulting in a burner equivalence ratio difference of $\Delta\phi \approx 0.05$ should be sufficient that the combustion system meets the $NO_x$ as well as the CO requirements for the whole operating range and fuels from natural gas to biogas with up to 50 % $CO_2$ content, and is therefore suitable to support the transition from conventional to a more sustainable power and heat production.

## ACKNOWLEDGEMENTS

The authors would like to thank Andreas Mader, Jürgen Roth, Timo Lingstädt, Stefan Hasemann, Teresa Siebel, Andreas Huber, Torsten Methling and Thiemo Reimers for the fruitful discussions and the support before and during the measurement campaigns.

## REFERENCES

[1] Fraunhofer-Institut für Solare Energieforschung ISE, 2019. Energy Charts.

[2] Reppich, M., Datzmann, S., Li, X., Rosenbauer, S., Schlecht, C., and Tschepur, S., 2009. "Vergleich verschiedener Aufbereitungsverfahren von Biogas zur Einspeisung in das Erdgasnetz". *Chemie Ingenieur Technik,* **81**(3), pp. 211–223.

[3] Zornek, T., Mosbach, T., and Aigner, M., 2018. "Optical Measurements of a LCV-Combustor Operated in a Micro Gas Turbine With Various Fuel Compositions". *Engineering Gas Turbines Power,* **141**(4).

[4] Wünning, J., and Wünning, J., 1997. "Flameless Oxidation to Reduce Thermal NO-Formation". *Progress in Energy and Combustion Science,* **23**(1), pp. 81–94.

[5] Cavaliere, A., and de Joannon, M., 2004. "Mild Combustion". *Progress in Energy and Combustion Science,* **30**, pp. 329–366.

[6] Lammel, O., Stöhr, M., Kutne, P., Dem, C., Meier, W., and Aigner, M., 2011. "Experimental Analysis of Confined Jet Flame by Laser Measurement Techniques". In Proceedings of ASME Turbo Expo, GT2011-45111.

[7] Zornek, T., Monz, T., and Aigner, M., 2013. "Experimentelle Charakterisierung eines Holzgas-Brenners für Mikrogasturbinen". In 26. Deutscher Flammentag, Vol. 2161, pp. 775–779.

[8] Zornek, T., Monz, T., and Aigner, M., 2013. "A Micro Gas Turbine Combustor for the use of Product Gases from Biomass Gasification". In Proceedings of the European Combustion Meeting 2013.

[9] Zornek, T., Monz, T., and Aigner, M., 2014. "Effizient, flexibel, sauber - FLOX®-Brennkammersysteme für Mikrotasturbinen". *BWK,* **66**(9), pp. 13 – 16.

[10] Zanger, J., Monz, T., and Aigner, M., 2013. "Progress in Gas Turbine Performance". *InTech, ch. Experimental Investigation of the Influence of Combustor Cooling on the Characteristics of a FLOX®-Based Micro Gas Turbine Combustor*, pp. 165–184.

[11] Zanger, J., Monz, T., and Aigner, M., 2015. "Experimental Investigation of the Combustion Characteristics of a Double-Staged FLOX®-Based Combustor on an Atmospheric and a Micro Gas Turbine Test Rig". In ASME Turbo Expo 2015: Turbine Technical Conference and Exposition, American Society of Mechanical Engineers.

[12] Bower, H. E., Grimm, F., Schwärzle, A., Roth, J., Zornek, T., and Kutne, P., 2018. "Experimental Analysis of the Fuel Flexibility of a Jet-Stabilized Micro Gas Turbine Combustor Designed for Low Calorific Gases". In Proceedings of GPPS-2018-0012.

[13] Seliger, H., Huber, A., and Aigner, M., 2015. "Experimental investigation of a flox®-based combustor for a small-scale gas turbine based chp system under atmospheric conditions". In ASME: GT2015-43094.

[14] Gohl, I., 2015. Experimentelle Untersuchung der Sensibilität des Brennverhaltens auf verschiedene Erdgasqualitäten und Vormischgüten in einem FLOX® Gasturbinen Brenner.

[15] Dandy, D., and Vosen, S., 1992. "Numerical and Experimental Studies of Hydroxyl Radical Chemiluminescence in Methane-Air Flames". *Combustion Science and Technology,* **82**, pp. 131–150.

[16] Nori, V. N., 2008. "Modeling and Analysis of Chemiluminescence Sensing for Syngas, Methane and Jet-A Combustion". PhD thesis, Georgia Institute of Technology.

[17] Seliger-Ost, H., 2019. "Entwicklung eines FLOX®-basierten Brennersystems für eine rekuperierte Mikrogasturbine im kleinen Leistungsbereich". PhD thesis, University of Stuttgart.

[18] Federal Ministry for Environment, Nature Conservation and Nuclear Safety, 2002. First General Administrative Regulation Pertaining the Federal Emission Control Act (Technical Instructions on Air Quality Control – TA Luft).

[19] Lefebvre, A. H., 1999. *Gas Turbine Combustion*. New York: CFC Press.

[20] Joos, F., 2006. *Technische Verbrennung – Verbrennungstechnik, Verbrennungsmodellierung, Emissionen*. Springer-Verlag.

[21] Biagioli, F., and Güthe, F., 2007. "Effect of pressure and fuel-air unmixedness on $NO_x$ emissions from industrial gas turbine burners". *Combustion and Flame,* **151**, pp. 274–288.

[22] Burdet, A., Lachaus, T., de la Cruz García, M., and Winkler, D., 2010. "Combustion under Flue Gas Recirculation Conditions in a Gas Turbine Lean Premix Burner". In Proceedings of ASME Turbo Expo, GT2010-23396.

[23] Ranzi, E., Frassoldati, A., Stagni, A., Pelucchi, M., Cuoci, A., and Faravelli, T., 2014. "Reduced Kinetic Schemes of Complex Reaction Systems: Fossil and Biomass-Derived Transportation Fuels". *International Journal of Chemical Kinetics,* **46**(9), pp. 512–542.

[24] Ranzi, E., Cavallotti, C., Cuoci, A., Frassoldati, A., Pelucchi, M., and Faravelli, T., 2015. "New Reaction Classes in the Kinetic Modeling of Low Temperature Oxidation of n-Alkanes". *Combustion and Flame,* **162**(5), pp. 1679–1691.

[25] Bagheri, G., Ranzi, E., Pelucchi, M., Parente, A., Frassoldati, A., and Faravelli, T., 2020. "Comprehensive Kinetic Study of Combustion Technologies for Low Environmental Impact: MILD and OXY-fuel Combustion of Methane". *Combustion and Flame,* **212**, pp. 142–155.

[26] Visser, W. P. J., Shakariyants, S. A., de Later, M. T. L., Haj Ayed, A., and Kusterer, K., 2012. "Performance Optimizaiton of a 3 kW Microturbine for CHP Application". In Proceedings of ASME Turbo Expo, GT2012-68686.

[27] Warnatz, J., Maas, U., and Dibble, R., 2006. *Combustion: Physical and Chemical Funda-*

*mentals, Modeling and Simulation, Experiments, Pollutant Formation*. Springer-Verlag.

## LIST OF FIGURES

## LIST OF TABLES